Research Article | Vol. 10, No. 10 / 1 October 2019 / Biomedical Optics Express 5414
Biomedical Optics EXPRESS

Co-cultured microfluidic model of the airway optimized for microscopy and micro-optical coherence tomography imaging

ZHONGYU LIU,[1,2] STEPHEN MACKAY,[1,2] DYLAN M. GORDON,[3] JUSTIN D. ANDERSON,[1,2] DUSTIN W. HAITHCOCK,[3] CHARLES J. GARSON,[3] GUILLERMO J. TEARNEY,[4] GEORGE M. SOLOMON,[2,5] KAPIL PANT,[3] BALABHASKAR PRABHAKARPANDIAN,[3] STEVEN M. ROWE,[1,2,5] AND JENNIFER S. GUIMBELLOT[1,2,*]

[1]*Department of Pediatrics, University of Alabama at Birmingham, Lowder Building Suite 620, 1600 7th Avenue South, Birmingham, AL 35233, USA*
[2]*Gregory Fleming James Cystic Fibrosis Research Center, University of Alabama at Birmingham, MCLM 706, 1918 University Blvd, Birmingham, AL 35294, USA*
[3]*Biomedical Technology, CFD Research Corporation, 701 McMillian Way NW, Huntsville, AL 35806, USA*
[4]*Department of Pathology, Wellman Center for Photomedicine, Massachusetts General Hospital, & Harvard Medical School, 55 Fruit St., Boston, MA 02114, USA*
[5]*Department of Medicine, University of Alabama at Birmingham, THT 422, 1900 University Blvd, Birmingham, AL 35294, USA*
[*]*jguimbellot@peds.uab.edu*

Abstract: We have developed a human bronchial epithelial (HBE) cell and endothelial cell co-cultured microfluidic model to mimic the *in vivo* human airway. This airway-on-a-chip was designed with a central epithelial channel and two flanking endothelial channels, with a three-dimensional monolayers of cells growing along the four walls of the channel, forming central clear lumens. These cultures mimic airways and microvasculature *in vivo*. The central channel cells are grown at air-liquid interface and show features of airway differentiation including tight-junction formation, mucus production, and ciliated cells. Combined with novel micro-optical coherence tomography, this chip enables functional imaging of the interior of the lumen, which includes quantitation of cilia motion including beat frequency and mucociliary transport. This airway-on-a chip is a significant step forward in the development of microfluidics models for functional imaging.

1. Introduction

Airways diseases, such as asthma, cystic fibrosis (CF), and chronic obstructive pulmonary disease (COPD), represent a major healthcare burden. COPD accounts for over $40 billion in annual healthcare costs [1] and recently surpassed stroke as the third leading cause of death in the United States [2] Asthma is a common chronic respiratory disease, affecting millions of adults and children worldwide. [3] CF is a genetic disease that limits lifespan, primarily due to respiratory complications, with no known cure. [4]. Despite the burden of these and other chronic respiratory diseases on the lives of millions of people worldwide, the study of basic pathophysiology, development of new therapeutics, and understanding of individual phenotypic variation to apply personalized approaches have been limited by the availability of appropriate airway models. *In vitro* models derived from human airway epithelia are particularly attractive because a robust monolayer of epithelial cells can be repeatedly generated from donated human airway epithelial cells. [5–7] However, replicating the airways, particularly the small airways, and recapitulating the *in vivo* environment remains challenging. Currently, the gold-standard *in vitro*

#371271 https://doi.org/10.1364/BOE.10.005414
Journal © 2019 Received 12 Jul 2019; revised 12 Sep 2019; accepted 20 Sep 2019; published 30 Sep 2019

Biomedical Optics EXPRESS

model of airway epithelia is the cell monolayer at air-liquid interface. [5] Most commonly, airway epithelial cells are grown in a static environment on a suspended membrane with cell culture media on the bottom, basolateral side, and air on the top, apical side. While useful for a variety of applications, this model does not fully replicate the *in vivo* physiologic environment and also represents a single cell type whereas the human airway epithelium is a complex organ including epithelial cells, endothelial cells, and fibroblasts, among others. Recently, microfluidics-based airway-on-a-chip models have been developed to overcome several of these limitations by adding features to improve dynamic flow and co-culture of endothelial cells. [8–14] These chips may also be miniaturized, potentially reducing the logistical burden for the source material of primary epithelial cells, and are often made of materials that are soft and pliable, allowing for simulation of normal breathing and shear stress. However, as yet, these airway models are still planar cultures grown at air-liquid interface and do not represent a complete tubular structure mirroring that of the airway.

We have developed a novel airway-on-a-chip model, using epithelial and endothelial co-cultures grown in a tubular structure. This chip produces an intact endothelial monolayer that grows on all four sides of a PDMS-based scaffold (vascular channel), with a central lumen through which air may flow (tissue channel). The central lumen communicates via pores to the two flanking vascular channels cultured with living endothelium around a central lumen filled with fluid, mimicking blood flow. All three channels may be accessed via ports at either end in order to conduct experiments. Together, this parallel tube design allows for an *in vitro* 3-dimensional hollow airway lumen with continuous airflow with two *in vitro* 3-dimensional microvascular structures comprised of intact endothelial layers. In addition, this chip was optimized for imaging, using coverslip optical glass as the base and thin layers of PDMS through which live-cell imaging may be conducted using traditional microscopy. Our novel micro-optical coherence tomography (μOCT) allows functional imaging for direct quantitation of ciliary movement, fluid movement, and particle tracking simultaneously *in vitro.* [15,16] A number of emerging studies suggest that mucociliary function, airway surface liquid, mucus secretion, and ciliary function are key downstream measures of upstream defects including CFTR dysfunction. [15,17,18] The use of μOCT to analyze tissue culture from individual subjects has the potential to characterize chronic respiratory disease phenotypes, improve understanding of basic pathophysiology of a variety of airways diseases, and aid in the development of new therapeutics that may be tested systemically (through the endothelial channels) or via inhalation (through the airway channel), while at the same time measuring downstream effects of interventions using functional imaging. The combination of an *ex vivo*, personalized cell-culture based organ model with full assessment of parameters of airway homeostasis via μOCT represents a new approach to personalized medicine in pulmonary disease.

2. Materials and methods

2.1. Device design and fabrication

The device comprises of a plastic, disposable and optically clear microfluidic chip that contains a central chamber for 3D culture of epithelial cells surrounded by endothelial cells. To achieve the *in vivo* physiological environment of lung architecture, the device was designed as shown in the conceptual schematic Fig. 1(a). In typical configuration, the vascular channels are 250 μm wide while the epithelial cells channel is 500 μm wide with a height of 100 μm mimicking the airway vessels. The fenestrations between the vascular channels and the airway channel that allow communication between the epithelial and endothelial cells were set at a cross-section of 5 μm × 5 μm with length of 50 μm. These fenestrations are very similar to the pores used in traditional transwells, except that the membrane is oriented vertically, to the side of the lumen, instead of at the bottom of the wells. We have used similar methodologies for fabrication vascular and tissue chambers communicating via porous architecture in several of our studies. [19–24]

Biomedical Optics EXPRESS

The porous interface is structured on SU-8 photoresist by patterning an extra layer in addition to the fluidic layer, which contained the fenestrations, channels and access port holes to form the communication layer between the airway and the vascular channels. Through holes, defining the inlets and outlets were punched using a 1.5 mm biopsy punch. Tygon Microbore tubing served as the connecting ports for fluidic interface. Figure 1(b) shows the fabricated device highlighting the pores of the channels.

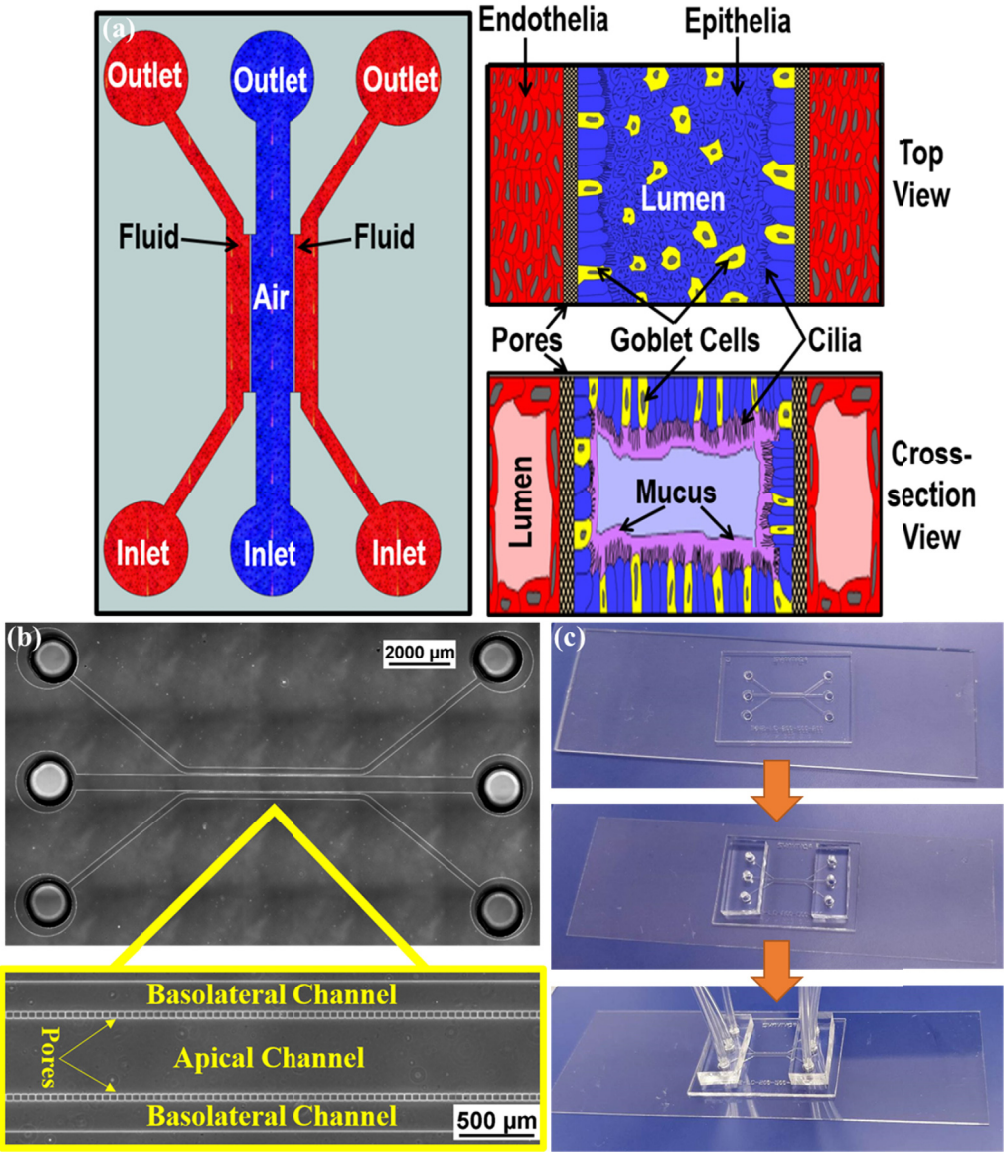

Fig. 1. (a) Schematic of the device to develop the air-liquid interface across the cells. The air (or epithelial) channel is separated from two fluid (basolateral) channels by pores. Right panel shows conceptual drawing of the proposed orientation of the cells when seen from top (above) and a cross-section (below). (b) Bright Field image of the fabricated device without cells and the magnified view showing the pores. (c) Fabricated device bonded to the glass coverslip with inserted tubing for perfusion.

Biomedical Optics EXPRESS

2.2. Device testing

The fabricated device was tested for fluidic integrity and pore integrity using fluorescent dextran and fluorescent particles. Figure 2(a) shows image of the device perfused with FITC-dextran while Fig. 2(b) and 2(c) shows images of the device following perfusion with 2 µm and 10 µm particles. As can be seen from the images, the devices are completely intact with no leakiness. In addition, while 2 µm particles are able to freely diffuse across the pores, the 10 µm particles are not able to cross the pores indicating a fully functional pore.

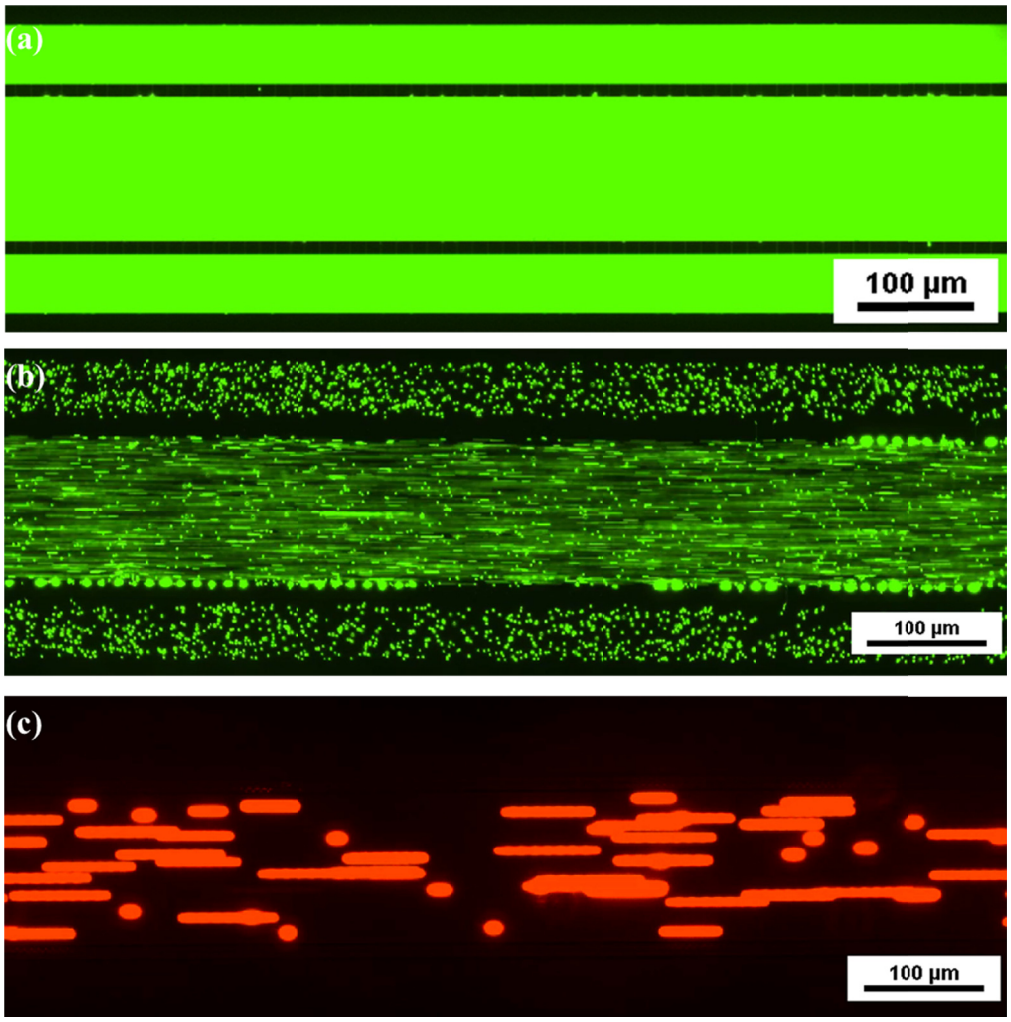

Fig. 2. Fluidic Integrity and Pore Integrity Testing. (a) FITC dextran perfused device indicating no leaks. (b) 2 µm particles readily permeate across the pores. (c) 10 µm particles unable to permeate across the pores indicating the functional pores as designed.

2.3. Cell expansion

In brief, our culturing methods are adapted from the well-known air-liquid interface culture method. [15,16] Human bronchial epithelial cells (HBEs) were initially obtained from the CF center of the University of Alabama at Birmingham under a protocol approved by the Institutional Review Board (IRB-151224002). All the cells were expanded via a co-culturing method with

Biomedical Optics EXPRESS

irradiated fibroblasts in F-media [17] for 10 days. The cells were harvested from co-culture using double trypsinization method and counted via hemocytometer. Human microvascular endothelial cells (HMEC) (Lonza, Cat. # CC-2527) were cultured in EGM-2MV medium with BulletKit (Lonza, Cat. # CC-3202).

2.4. Chip preparation

Tygon tubing was inserted into all six ports of the microfluidic chip. The center channel of the microfluidic chips was coated with type IV Human Placental Collagen (HPC) (Sigma, Cat. # C5533-5MG) to help cell attachment. Briefly, 50 µg/mL of HPC was slowly injected by hand, using a 1 mL syringe until the outlet port tubing is filled. All the tubing was cut to the equal length and closed using a tube clamp. The device was incubated at 4°C overnight. The following day, all the channels were thoroughly rinsed with PBS, then refilled with F-media. The device was placed into the cell culture incubator at 37°C till use. Before seeding the cells, all the channels were washed once with the media used for the following cell culture.

2.5. Cell culture in the chips

The airway epithelial cells were seeded into the center channel at a density of 3–4×10^4 cells/µL via tubing and then the tubing was clamped to allow the cells to settle in the channel at 37°C for 5 hours. After the cells attached to the channel, all three channels were connected using the tubing to a syringe pump (PHD Ultra, Harvard Apparatus) and ran F-media through them at a rate of 3 µL/min for 4 minutes every 6 hours. After 2–3 days, the media was changed to differentiation media using Ultroser-G based media [15] and media flowed through all 3 channels for 1 day, followed by media via only through center channels at a rate of 0.5 µL/min for 4 hours, then off 4 hours, with the cycle repeated for 3 days. Media flow was switched through two vascular channels and the center channel tubing was connected to an air pump (Precision Medical EasyAir PM15) with a low flow-rate regulator to introduce humidified room air; flow rate was adjusted to the minimal flow (indicated by continuous bubbling in humidification bottle) to maintain air-liquid interface (ALI). Air from the compressor was pumped via tubing into a bottle containing differentiation media. The media-humidified air was then directed into the devices. Flow was controlled using a high precision flow controller (McMaster-Carr, Cat. # 46425K22) that was connected to the compressor. This air-liquid interface culture system was maintained for up to 14 days.

After the airway epithelial cells were differentiated for 7 days, HMEC cells were then seeded into the vascular channels to establish the co-culture model. The HMEC cells were seeded and maintained under a continuous perfusion condition as described previously. [18,22,25] The co-culture system was retained for further 7 days until endpoint assays were performed. The chips were cultured in an incubator containing 5% CO_2 and at 85–95% humidity at 37°C. The media and tubing for the vascular channels were changed 2–3 times per week.

2.6. Viability assay and immunofluorescence

Viability assays were performed using live/dead assay kit (Fisher Scientific, Cat. # L3224). The solution containing Calcein AM and Ethidium Homodimer-1 was injected into the devices and incubated for 30 minutes. Following a flush, the devices were imaged using fluorescence microscopy. The live cells were imaged at 488 nm and the dead cells were imaged at 598 nm. Living cells were also imaged using Plasma Membrane Orange (ThermoFisher, Cat. # C10045) and Calcein Green (ThermoFisher, Cat. # C34852). Immunofluorescence staining was performed following methods described previously [26–28]. Briefly, the cells were washed by flowing PBS through all three channels, fixed with 4% paraformaldehyde (Electron Microscopy Sciences, USA) for 10 min at room temperature (RT), and washed gently by flowing additional PBS. The cells were permeabilized by 0.01% Triton X-100 (Alfa Aesar, Cat. # A16046) for 10 minutes

Biomedical Optics EXPRESS

at RT. After washing with PBS, the cells were blocked with 1% BSA in PBS (ThermoFisher, Cat. # BP1600-100) for 1 hour at room temperature. Following washing, primary antibodies were introduced into the appropriate channels followed by secondary antibodies. All primary and secondary antibody solutions were prepared with 1% BSA. Primary antibody incubation was carried out overnight at 4°C. All secondary antibodies from Jackson ImmunoResearch were diluted at 1:400 in 1% BSA and incubated at room temperature for 60 minutes. After incubation, the channels were washed thoroughly with PBS. NucBlue (Invitrogen, Cat. # R37605) in PBS was injected into the devices for nuclear staining. The chips were then imaged with either an inverted microscope (Nikon Ts2) or a confocal microscope (Nikon A1R-HD25). The primary antibodies used are as following: anti-human ZO1/TJP1 for tight junctions (ThermoFisher, Cat. # 44–2200, 1:100), anti-human E-Cadherin for intercellular junctions (Millipore, Cat. # MAB3199, 1:20), anti-human VE-Cadherin for endothelial cell junctions (R&D Systems, Cat. # AF938, 1:50).

2.7. μOCT functional assay

Micro-optical coherence tomography (μOCT) images were constructed using the standard Fourier-domain image reconstruction techniques [29]. The methods previously described [30] were used to quantify the respiratory epithelial functional parameters of ciliary beat frequency (CBF) and mucociliary transport rate (MCT).

Chips were removed from the incubator by disconnecting all the tubing connected with the pump and air compressor, and imaged immediately. The chips were placed into an environmental chamber which controls temperature (37°C), CO_2 gas (5%), and humidification. The environmental chamber was rotated to enable imaging of the chip through the coverslip side. After properly positioning the chips, all the reagent solutions and beads (for flow visualization and analysis) were slowly and gently injected into the appropriate channels through the tubing. After administration of reagents to the vascular channels, the syringes remained connected to the tubing of the inlet port to maintain pressure equilibrium. The syringe connected to the tubing of the inlet port of the central channel was removed and clamped to eliminate movement of fluid due to atmospheric pressure and avoid false elevation of MCT. Incubation for approximately 10 minutes allowed equilibration of air and fluid flow in the chips after these setup procedures prior to acquiring images.

CBF and MCT were determined from images sequences compiled of at least 250 frames taken at 40 frames/second. Using a Matlab script developed previously [30], CBF was measured by drawing a line over the area that represents the surface of the epithelium. This script computes CBF based on analyzing the pixels that express the sharpest Fourier peaks. Regions of interest were scanned for ciliary activity. Areas of ciliary activity were marked with a line over the surface of epithelium. The script automatically identifies five to ten areas to quantify ciliary beat frequency. CBF data was further processed by setting more stringent thresholds to exclude motion artifact as follows: CBF data with confidence levels less than 0.7 and/or peaks that did not reach a power spectral density of 3×10^7 or higher were excluded from the analysis. The CBF confidence level represents how clean the peaks are, and more rigorous thresholds allowed the elimination of low confidence peaks. After this quality control, all CBF values from all regions of interest were averaged and standard deviation calculated. MCT was quantified in Image J by measuring the displacement of 5–10 visible beads in the central lumen through time as described previously. [30] Briefly, this quantification was performed by drawing a line in the lumen of the chip parallel to the direction of transport, for which an intensity along this line was represented as a function of time displayed as a 2D image. In this 2D image movement of beads or particles was seen as a slanted streak (see Appendix, Fig. 8). The slope of this streak was then used to calculate the velocity of the moving object, similarly described in other particle streak velocimetry methods. Data was represented using GraphPad Prism 7 (San Diego, CA).

Biomedical Optics EXPRESS

3. Results

3.1. Human airway epithelial cell growth in the chips

Primary human bronchial epithelial cells (HBECs) were seeded into the chips at density 3–4×10^4 cells/μL. The cells were then allowed to attach to the bottom of the chips in the cell culture incubator at 37°C for 5 hours and further cultured for 7 days as described in the materials and methods. Figure 3(a-c) show viable and confluent cells in the chips over time. To assess the viability of the cells, live/dead assays were performed. Highly viable cells were observed in the chips (Fig. 3(d)). To further confirm whether the cells can expand to all four walls of the chips to form an airway-like tube, CellMask orange plasma membrane stain and Calcein green, AM were used to visualize the cell membrane and cytoplasm in the living cells (Fig. 3(e)and 3(f)). Confocal 3D reconstruction pictures identified the HBECs formed an intact lumen in the chips with nearly 100% confluence of the cells on the walls (Fig. 3(e)and 3(f)).

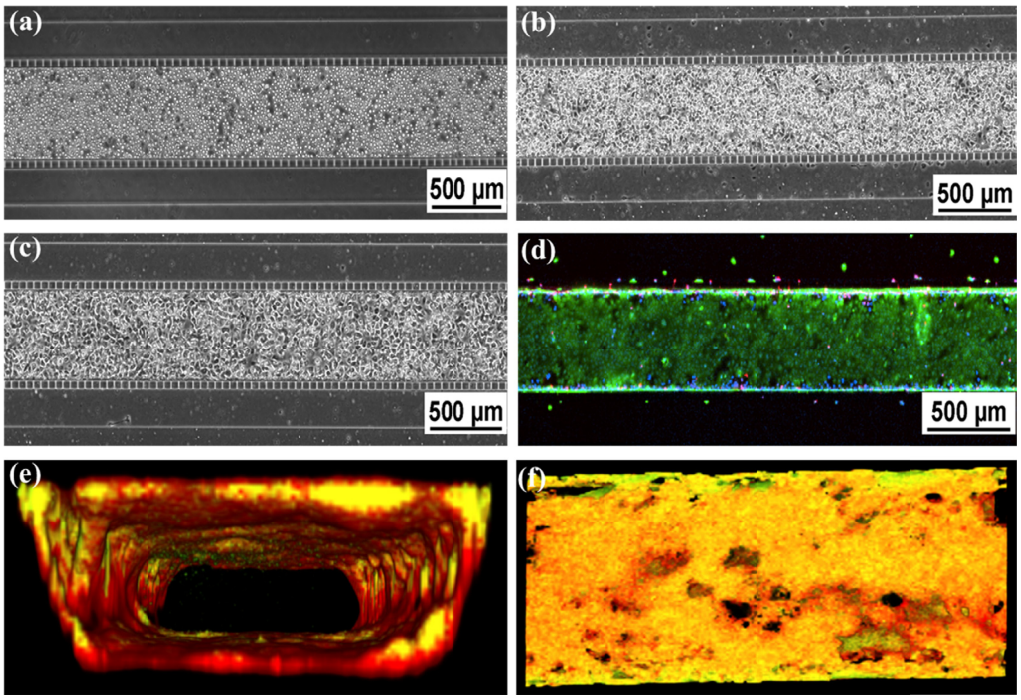

Fig. 3. Confluence and Viability of Epithelial Cell Culture. (a-c). Phase contrast imaging of HBE cells in the center channel: (a) Directly after seeding, (b) attachment of cells after 24 hours, and (c) 100% confluence after 7 days of culture. (d) Live/dead staining. (e) Cross-sectional view of 3-D reconstructed confocal image (10X mag.). Cell culture is co-stained with Plasma Membrane Orange and Calcein Green. (f). *En face* of Fig. 3(e).

3.2. Co-culture system of human airway epithelial and endothelial cells in the chips

To mimic the *in vivo* human airway, we co-cultured the human bronchial epithelial cells and endothelial cells in the chips. As described in the materials and methods, the endothelial cells were introduced into the two side channels after the HBE cells were growing in the center channel for 7 days. Figure 4(a) and 4(b) show the cells reach 100% confluence in all three channels. To further investigate the morphology of these cultures in the three-channel configuration, a video was taken from one side to the other of the chips by Nikon Ts2. To clearly show the cells, the

Biomedical Optics EXPRESS

nuclei was stained with Nucblue. 100% confluence of the cells were identified in both top and bottom walls in the center channel as well as two side channels (Fig. 4(c) and Visualization 1). Furthermore, confocal 3D reconstruction also confirmed the lumen formed both in the center channel and two side channels (Fig. 4(d)).

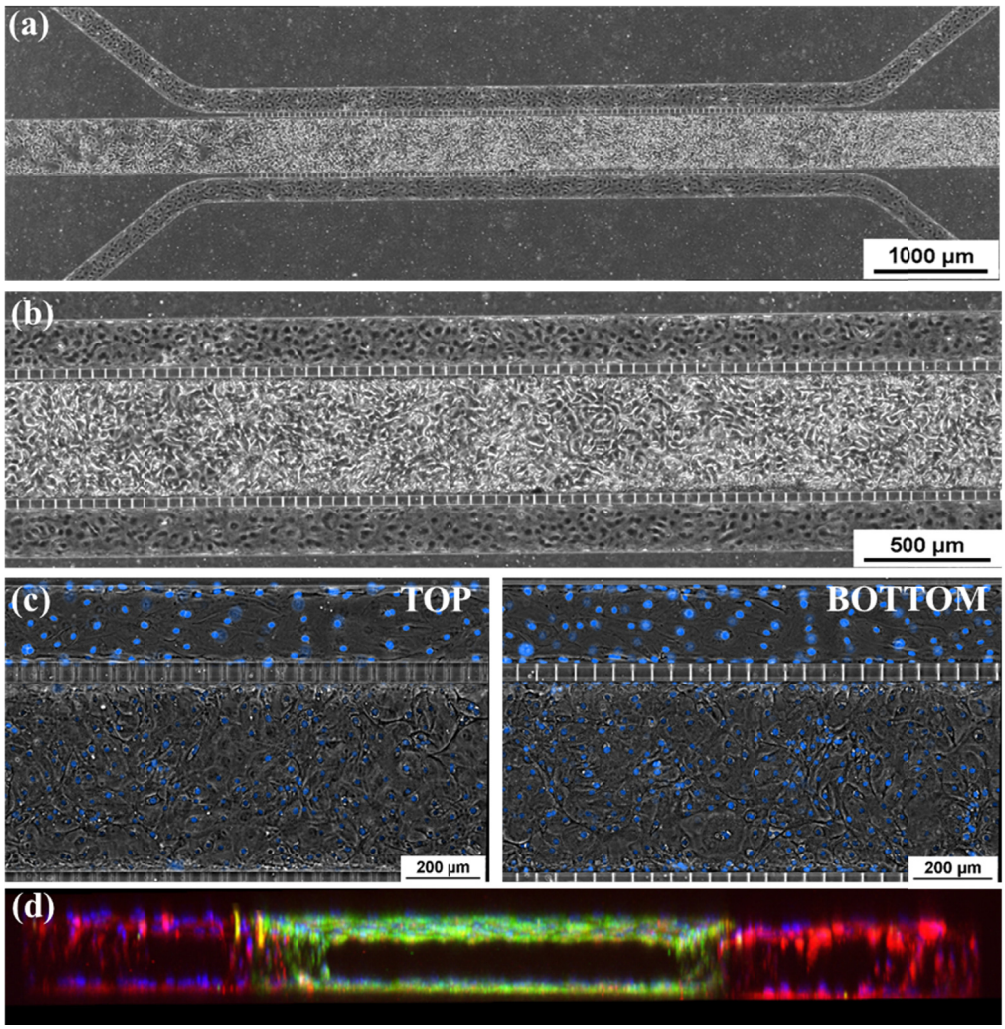

Fig. 4. Epithelial and Endothelial Co-Culture in Microfluidic Chip. (a) and (b) Phase Contrast image of confluent co-cultured chip with epithelial cells in the center channel and endothelial cells lining the peripheral channels. (c) Phase Contrast of top and bottom of the channel showing confluent monolayers in tissue and vascular channel. The full imaging from top to bottom is shown in Visualization 1. These images show the confluence of cells on both the top and bottom of the center channel and one side channel with a central, clear lumen. (d) Cross-sectional, 3-D reconstructed confocal image of co-cultured chip showing lumen formation in all three channels (10X mag.).

3.3. Fully differentiated human bronchial epithelial cells in the chips

To test whether the HBE cells are fully differentiated in the chips, several airway epithelial markers were investigated in the cells by immunofluorescence staining. ZO-1 is a key protein

Biomedical Optics EXPRESS

in tight junction that is one of epithelial cell junctions in vertebrates. [26] E-Cadherin is a crucial component for formation of tight junctions in human bronchial epithelial cells. [31,32] VE-Cadherin is a major protein component of intercellular junctions between cells of the endothelium. [23,33] Both ZO-1 and E-Cadherin were detected in the HBEs of the center channel (Fig. 5(a) and (b)); Visualization 2). VE-Cadherin was seen in the endothelial cells of two side channels (Fig. 5(a) and 5(b); Visualization 2). Muc5AC is a major mucin secreted by airway goblet cells. [34] It was identified in the cells of the epithelial channel (Fig. 5(c)). Figure 5(d) showed the cilia on the cell surface in the epithelial channel (also see Visualization 3). The combination of differentiated airway epithelium in the center channel as well as the endothelial cells in the peripheral side channels represents an airway-like environment and architecture.

3.4. Functional assay with micro-optical coherence tomography for the chips

To assess the functional characteristics of airway epithelial cells, we adapted the previously developed micro-optical coherence tomography (μOCT) method. [30,35,36] This method also allows us to visualize the confluence and architecture of the differentiated airway cells with both cross-section and transverse views of the channel (Fig. 6; Visualization 4) and Visualization 5). The cross-sectional views (Fig. 6(b) and 6(c)) confirm growth of airway cells forming a complete tube-like structure similar to the lumen seen in the airways. Transverse imaging confirms that cellular growth occurs on both sides of the chip (Fig. 6(d) and (f)) as well as the top and bottom but not in the lumen (Fig. 6(e)).

Airway epithelial functional characteristics can also be measured such as ciliary beat frequency (CBF) and mucociliary transport (MCT) (Fig. 7). Ciliary dysfunction has been described in many airway diseases [37,38], thus these parameters are important to measure. The function of cilia can be evaluated by measuring the movement of cilia and their ability to move mucus and particles along the airway. MCT can also be affected by the viscosity of mucus in the airway such as diseases like CF. [39,40] Along the surface of the epithelium, the beat frequency of cilia can be measured (Fig. 7(a) and (b)). To measure MCT, micro-beads are introduced into the center channel to represent particulates that would be transported along the airway *in vivo*. After equilibration, the velocity of bead movement down the channel is measured over time (Fig. 7(c) and 7(d); Visualization 6 and Visualization 7). Three replicate chips were used for imaging. From each chip, 3–4 unique regions of interest were imaged for a total of ten regions. In each region, 5–10 measurements for MCT and CBF were made. These measurements were averaged to produce a single mean value for each region (displayed in Fig. 7(e). In one region, measurements for CBF did not meet our strict quality control thresholds (described in the methods section 2.7) and thus only nine measurements are displayed.

Biomedical Optics EXPRESS

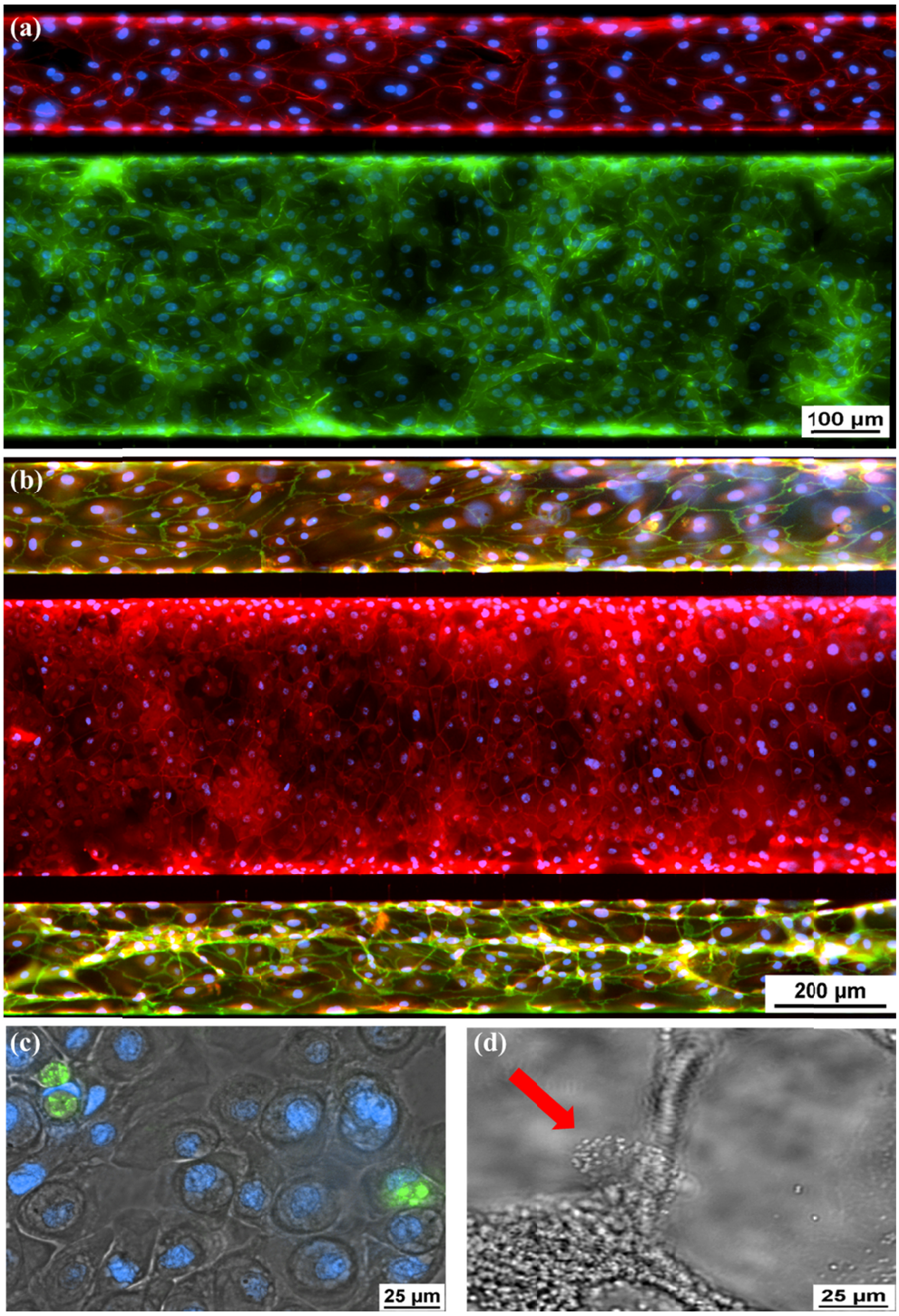

Fig. 5. Immunofluorescence of Differentiated Epithelial and Endothelial Cells. (a) E-cadherin (green), epithelial cell adherin protein. VE-Cadherin (red), endothelial cell adherin protein. The full imaging from top to bottom is shown in Visualization 2. (b) ZO-1 (red) staining tight junctions of epithelial cells in central channel and also VE-Cadherin staining (green) in vascular channel. (c) Muc5ac (green), intracellular mucin staining inside of epithelial cells. (d) Ciliated epithelial cell indicated by the red arrow. Cilia beating shown in Visualization 3.

Biomedical Optics EXPRESS

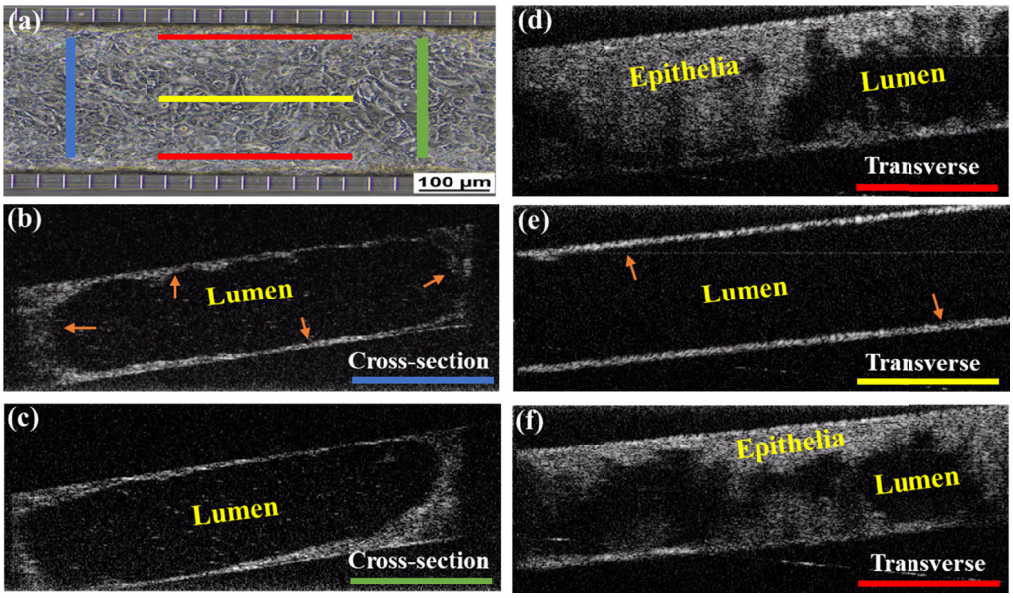

Fig. 6. Visualization of Primary Human Bronchial Epithelial (HBE) Cells in the Microfluidic Chip using µ-OCT. (a) Schematic for orientation of µ-OCT slices through the center channel. (b) Cross-sectional slice more proximal to fluid flow in the chip. Arrow head (orange) indicates epithelial cells and the black center represents the lumen. (c) Cross-sectional slice taken more distally. (d) Transverse slice showing the topography of a thick monolayer of epithelial cells along the walls of the chip. (e) Transverse slice in the center of the chip showing confluent layer of epithelial cells growing along the top and bottom surfaces (orange arrow). (f) Transverse slice of the opposite chip wall.

Biomedical Optics EXPRESS

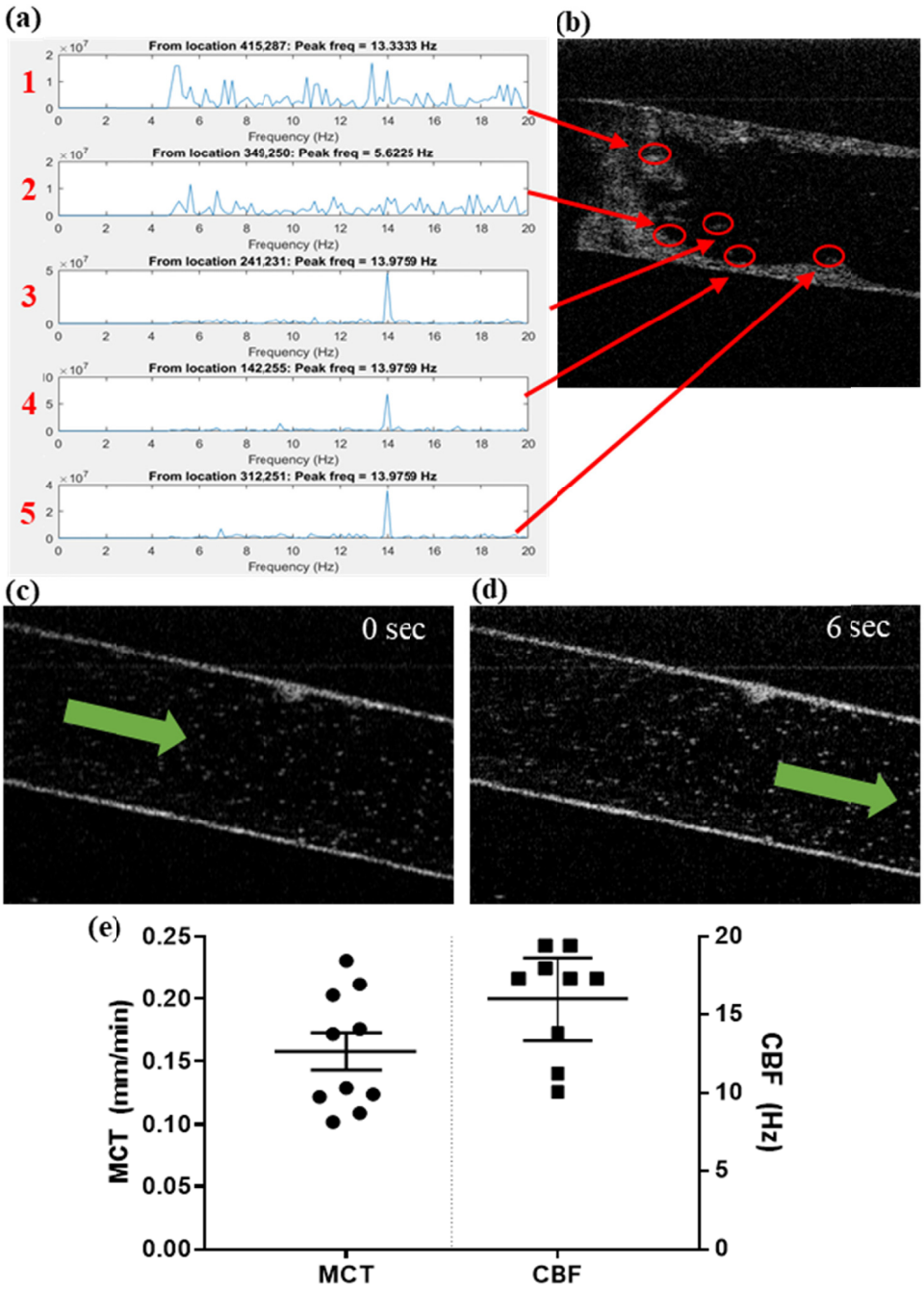

Fig. 7. Ciliary Beating Frequency (CBF) and Mucociliary Transport (MCT) Analysis using μ-OCT. (a) The frequency of peak amplitudes in the temporal Fourier transform of 5 regions. (b) 5 regions of interest (red circles) along the epithelial surface that detected oscillatory motion suggestive of cilia. (c) Transverse view in the lumen of the central epithelial channel. Mucociliary transport motion direction indicated by green arrow (see Visualization 7). (d) Still image 6 seconds later showing displacement of beads from their original location. (Visualization 7) (e) Recorded values for 3–4 regions of interest along the length of 3 replicate chips cultured with human bronchial epithelial cells. The average MCT (mm/min) and CBF (Hz) values for each of those regions are indicated by a filled circle or square, respectively.

Biomedical Optics EXPRESS

4. Discussion

The novel airway-on-a-chip described in this study represents a significant step forward in the development of microfluidics airway models. The chip design allows for epithelial cell culture which forms a central clear lumen for air or fluid flow, flanked on each side by endothelial channels which similarly grow around a central clear lumen for continuous fluid flow. To our knowledge, this is the first design that provides a framework for a 3-dimensional airway space surrounded by 3-dimensional endothelium, providing a new opportunity to model airway physiology. The accessibility of the proximal and distal ends of these channels make the model flexible for a variety of applications, including assessment of "systemic" versus "inhaled" delivery of therapeutic compounds. The development of the chip with PDMS as the primary scaffold could allow for manipulation of the lumens by altering pressure and stretch, similar to breathing. The combination of μOCT with this novel chip enables functional imaging of critical airway physiology in an intact lumen, which can further be personalized to individual patients. This airway model recapitulates many features of the human airway, with intact tight junctions, a variety of epithelial cell types including mucus-producing cells, and functional cilia, in a monolayer completely surrounding a lumen similar to an airway, which has never before been described. By extending the planar culture to a complete lumen, this model captures the key benefits of typical air-liquid-interface cultures while furthering the physiologic similarity to the human airway.

Specifically, the epithelial cells in a tubular structure enhance cell-to-cell contact that is crucial for inducing differentiation and coordinated mucociliary transport. This format increases the cell-to-cell contact in multiple directions and has the potential for improving differentiation and directionality of the cells, including ciliary beat. In the intact airway, cilia are organized and coordinated in a three-dimensional structure, enhancing mucociliary transport. In a planar culture, cell-to-cell contact is less in comparison, often yielding clusters of cilia that may be organized within that small area but lack coordination with other areas. As an additional benefit, MCT is based on cumulative transport by energy transferred from coordinated cilia movement. In planar cultures, laminar flow can break down under high mucus loads, and MCT is less efficient. [41] In 3 dimensional tubular airways, cilia can contribute to mucus transport from more than one angle, reducing non-laminar flow. As evidence of this, in intact airways and trachea, mean MCT rates are faster than *in vitro* planar cultures, [7,16,42] supporting the idea that a fully intact monolayer in a tubular *in vitro* airway may enhance differentiation, organization, and directionality above what planar cultures can achieve. To further replicate airway physiology, we incorporated tubular endothelial cultures, composed of highly differentiated cells growing under continuous flow conditions. [33,43–45] These cultures also mimic *in vivo* microvasculature including polarization and tight junction formation. [46,47] Combined with the *in vitro* airway lumen, this microfluidics chip provides an enhanced model for assessing normal and abnormal epithelial:endothelial relationships.

Our airway-on-a-chip model may be an important tool for research purposes, helping to understand basic pathophysiology of airways diseases, and for pharmaceutical development, as a pre-clinical tool to complement existing *in vitro* and animal models. This study is limited by restriction to human bronchial epithelial cells and human lung microvascular endothelial cells. However, pulmonary epithelial cells of any type could potentially be grown in this chip in a similar manner, including tracheal epithelia and alveolar epithelia. Future studies could investigate the use of this model for studying physiological responses including inflammation, inhalational toxicology of known toxicants and/or efficacy of medical countermeasures and therapeutic screening via respiratory drug delivery. Further, the model may be used to predict drug efficacy on an individualized basis as a personalized medicine tool. Also, linking of this airway model with other tissue types in a "human-on-a-chip" model, which will be particularly valuable for pharmacologic preclinical studies may also be explored.

Biomedical Optics EXPRESS

5. Conclusion

We have developed a novel microfluidic model of the airway that, by miniaturizing airways that are comprised of donor cells derived from patients, will provide an innovative means to replicate the airways *ex vivo*, enabling pharmacologic and mechanistic studies of the airway on a personalized basis.

Appendix

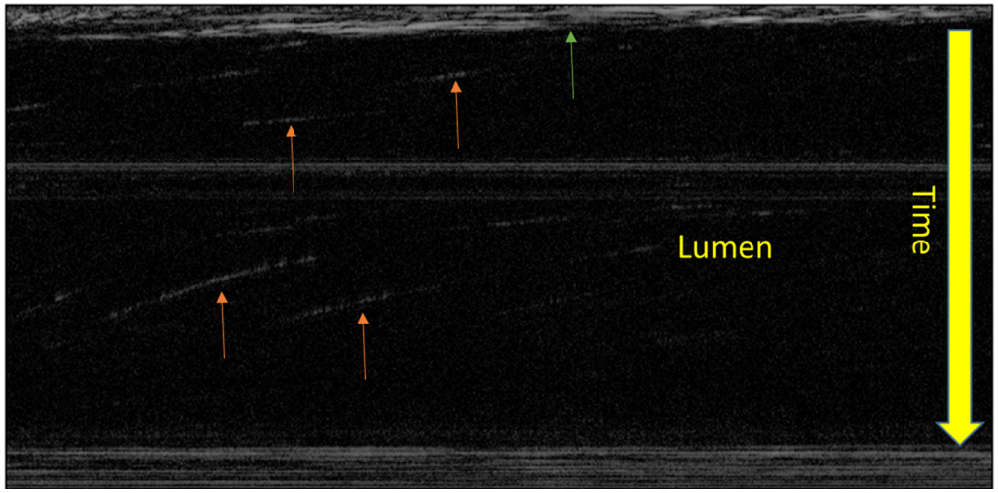

Fig. 8. MCT particle streak velocimetry analysis. This is the 2D representation of the displacement of beads over time. The orange arrows represent the movement of a bead for which the slope is used to calculate velocity. The green arrow is showing the epithelial surface.

Funding

National Heart, Lung, and Blood Institute (1R43HL134056-01, R35HL135816); National Institute of Diabetes and Digestive and Kidney Diseases (P30 DK072482); Cystic Fibrosis Foundation; Center for Clinical and Translational Science, University of Alabama at Birmingham (CCTS, UAB) (UL1TR001417); Mucus Clearance Consortium.

Acknowledgments

We would like to thank the following people for technical contributions to this manuscript: Hank Fortinberry, Marina Mazur, Lily Deng, Deborah Ramsey, and Hui Min Leung. Research reported in this publication was supported by the UAB High Resolution Imaging Facility and the UAB University-Wide Research Center Gregory Fleming James Cystic Fibrosis Center Clinical and Translational Core.

Disclosures

Dr. Rowe reports grants from Bayer (F), grants from Forest Research Institute (F), grants from AstraZeneca (F), grants from N30/Nivalis (F), grants from Novartis (F), grants from Galapagos/AbbVie (F), grants from Proteostasis (F), grants from Eloxx (F), grants and personal fees from Celtaxsys (F,C), grants from PTC Therapeutics (F), grants, personal fees and non-financial support from Vertex Pharmaceuticals Incorporated (F,C,S), personal fees from Bayer

Biomedical Optics EXPRESS

(C), personal fees from Novartis (C), personal fees from Renovion (C), outside the submitted work. All other authors declare no conflicts of interest. The microfluidic device will be available commercially from SynVivo Inc.

References

1. Morbidity and Mortality: 2007 Chart Book on Cardiovascular, Lung and Blood Diseases, pp 17, Chart 2-24, National Institutes of Health, National Heart Lung and Blood Institute
2. Centers for Disease Control and Prevention. National Center for Health Statistics. Final Vital Statistics Report. Deaths: Final Data for 2007. Vol. 58, No. 19, May 2010
3. T. Vos, A. D. Flaxman, M. Naghavi, R. Lozano, C. Michaud, M. Ezzati, K. Shibuya, J. A. Salomon, S. Abdalla, V. Aboyans, J. Abraham, I. Ackerman, R. Aggarwal, S. Y. Ahn, M. K. Ali, M. Alvarado, H. R. Anderson, L. M. Anderson, K. G. Andrews, C. Atkinson, L. M. Baddour, A. N. Bahalim, S. Barker-Collo, L. H. Barrero, D. H. Bartels, M. G. Basanez, A. Baxter, M. L. Bell, E. J. Benjamin, D. Bennett, E. Bernabe, K. Bhalla, B. Bhandari, B. Bikbov, A. Bin Abdulhak, G. Birbeck, J. A. Black, H. Blencowe, J. D. Blore, F. Blyth, I. Bolliger, A. Bonaventure, S. Boufous, R. Bourne, M. Boussinesq, T. Braithwaite, C. Brayne, L. Bridgett, S. Brooker, P. Brooks, T. S. Brugha, C. Bryan-Hancock, C. Bucello, R. Buchbinder, G. Buckle, C. M. Budke, M. Burch, P. Burney, R. Burstein, B. Calabria, B. Campbell, C. E. Canter, H. Carabin, J. Carapetis, L. Carmona, C. Cella, F. Charlson, H. Chen, A. T. Cheng, D. Chou, S. S. Chugh, L. E. Coffeng, S. D. Colan, S. Colquhoun, K. E. Colson, J. Condon, M. D. Connor, L. T. Cooper, M. Corriere, M. Cortinovis, K. C. de Vaccaro, W. Couser, B. C. Cowie, M. H. Criqui, M. Cross, K. C. Dabhadkar, M. Dahiya, N. Dahodwala, J. Damsere-Derry, G. Danaei, A. Davis, D. De Leo, L. Degenhardt, R. Dellavalle, A. Delossantos, J. Denenberg, S. Derrett, D. C. Des Jarlais, S. D. Dharmaratne, M. Dherani, C. Diaz-Torne, H. Dolk, E. R. Dorsey, T. Driscoll, H. Duber, B. Ebel, K. Edmond, A. Elbaz, S. E. Ali, H. Erskine, P. J. Erwin, P. Espindola, S. E. Ewoigbokhan, F. Farzadfar, V. Feigin, D. T. Felson, A. Ferrari, C. P. Ferri, E. M. Fevre, M. M. Finucane, S. Flaxman, L. Flood, K. Foreman, M. H. Forouzanfar, F. G. Fowkes, R. Franklin, M. Fransen, M. K. Freeman, B. J. Gabbe, S. E. Gabriel, E. Gakidou, H. A. Ganatra, B. Garcia, F. Gaspari, R. F. Gillum, G. Gmel, R. Gosselin, R. Grainger, J. Groeger, F. Guillemin, D. Gunnell, R. Gupta, J. Haagsma, H. Hagan, Y. A. Halasa, W. Hall, D. Haring, J. M. Haro, J. E. Harrison, R. Havmoeller, R. J. Hay, H. Higashi, C. Hill, B. Hoen, H. Hoffman, P. J. Hotez, D. Hoy, J. J. Huang, S. E. Ibeanusi, K. H. Jacobsen, S. L. James, D. Jarvis, R. Jasrasaria, S. Jayaraman, N. Johns, J. B. Jonas, G. Karthikeyan, N. Kassebaum, N. Kawakami, A. Keren, J. P. Khoo, C. H. King, L. M. Knowlton, O. Kobusingye, A. Koranteng, R. Krishnamurthi, R. Lalloo, L. L. Laslett, T. Lathlean, J. L. Leasher, Y. Y. Lee, J. Leigh, S. S. Lim, E. Limb, J. K. Lin, M. Lipnick, S. E. Lipshultz, W. Liu, M. Loane, S. L. Ohno, R. Lyons, J. Ma, J. Mabweijano, M. F. MacIntyre, R. Malekzadeh, L. Mallinger, S. Manivannan, W. Marcenes, L. March, D. J. Margolis, G. B. Marks, R. Marks, A. Matsumori, R. Matzopoulos, B. M. Mayosi, J. H. McAnulty, M. M. McDermott, N. McGill, J. McGrath, M. E. Medina-Mora, M. Meltzer, G. A. Mensah, T. R. Merriman, A. C. Meyer, V. Miglioli, M. Miller, T. R. Miller, P. B. Mitchell, A. O. Mocumbi, T. E. Moffitt, A. A. Mokdad, L. Monasta, M. Montico, M. Moradi-Lakeh, A. Moran, L. Morawska, R. Mori, M. E. Murdoch, M. K. Mwaniki, K. Naidoo, M. N. Nair, L. Naldi, K. M. Narayan, P. K. Nelson, R. G. Nelson, M. C. Nevitt, C. R. Newton, S. Nolte, P. Norman, R. Norman, M. O'Donnell, S. O'Hanlon, C. Olives, S. B. Omer, K. Ortblad, R. Osborne, D. Ozgediz, A. Page, B. Pahari, J. D. Pandian, A. P. Rivero, S. B. Patten, N. Pearce, R. P. Padilla, F. Perez-Ruiz, N. Perico, K. Pesudovs, D. Phillips, M. R. Phillips, K. Pierce, S. Pion, G. V. Polanczyk, S. Polinder, C. A. Pope 3rd, S. Popova, E. Porrini, F. Pourmalek, M. Prince, R. L. Pullan, K. D. Ramaiah, D. Ranganathan, H. Razavi, M. Regan, J. T. Rehm, D. B. Rein, G. Remuzzi, K. Richardson, F. P. Rivara, T. Roberts, C. Robinson, F. R. De Leon, L. Ronfani, R. Room, L. C. Rosenfeld, L. Rushton, R. L. Sacco, S. Saha, U. Sampson, L. Sanchez-Riera, E. Sanman, D. C. Schwebel, J. G. Scott, M. Segui-Gomez, S. Shahraz, D. S. Shepard, H. Shin, R. Shivakoti, D. Singh, G. M. Singh, J. A. Singh, J. Singleton, D. A. Sleet, K. Sliwa, E. Smith, J. L. Smith, N. J. Stapelberg, A. Steer, T. Steiner, W. A. Stolk, L. J. Stovner, C. Sudfeld, S. Syed, G. Tamburlini, M. Tavakkoli, H. R. Taylor, J. A. Taylor, W. J. Taylor, B. Thomas, W. M. Thomson, G. D. Thurston, I. M. Tleyjeh, M. Tonelli, J. A. Towbin, T. Truelsen, M. K. Tsilimbaris, C. Ubeda, E. A. Undurraga, M. J. van der Werf, J. van Os, M. S. Vavilala, N. Venketasubramanian, M. Wang, W. Wang, K. Watt, D. J. Weatherall, M. A. Weinstock, R. Weintraub, M. G. Weisskopf, M. M. Weissman, R. A. White, H. Whiteford, S. T. Wiersma, J. D. Wilkinson, H. C. Williams, S. R. Williams, E. Witt, F. Wolfe, A. D. Woolf, S. Wulf, P. H. Yeh, A. K. Zaidi, Z. J. Zheng, D. Zonies, A. D. Lopez, C. J. Murray, M. A. AlMazroa, and Z. A. Memish, "Years lived with disability (YLDs) for 1160 sequelae of 289 diseases and injuries 1990–2010: a systematic analysis for the Global Burden of Disease Study 2010," Lancet **380**(9859), 2163–2196 (2012).
4. D. Goetz and C. L. Ren, "Review of Cystic Fibrosis," Pediatr. Ann. **48**(4), e154–e161 (2019).
5. M. L. Fulcher and S. H. Randell, "Human nasal and tracheo-bronchial respiratory epithelial cell culture," Methods Mol. Biol. **945**, 109–121 (2013).
6. K. K. Chu, D. Mojahed, C. M. Fernandez, Y. Li, L. Liu, E. J. Wilsterman, B. Diephuis, S. E. Birket, H. Bowers, G. Martin Solomon, B. S. Schuster, J. Hanes, S. M. Rowe, and G. J. Tearney, "Particle-Tracking Microrheology Using Micro-Optical Coherence Tomography," Biophys. J. **111**(5), 1053–1063 (2016).
7. S. E. Birket, K. K. Chu, G. H. Houser, L. Liu, C. M. Fernandez, G. M. Solomon, V. Lin, S. Shastry, M. Mazur, P. A. Sloane, J. Hanes, W. E. Grizzle, E. J. Sorscher, G. J. Tearney, and S. M. Rowe, "Combination therapy with cystic

Biomedical Optics EXPRESS

fibrosis transmembrane conductance regulator modulators augment the airway functional microanatomy," Am. J. Physiol-Lung C **310**(10), L928–L939 (2016).
8. A. van den Berg, C. L. Mummery, R. Passier, and A. D. van der Meer, "Personalised organs-on-chips: functional testing for precision medicine," Lab Chip **19**(2), 198–205 (2019).
9. J. Tenenbaum-Katan, A. Artzy-Schnirman, R. Fishler, N. Korin, and J. Sznitman, "Biomimetics of the pulmonary environment in vitro: A microfluidics perspective," Biomicrofluidics **12**(4), 042209 (2018).
10. M. Humayun, C. W. Chow, and E. W. K. Young, "Microfluidic lung airway-on-a-chip with arrayable suspended gels for studying epithelial and smooth muscle cell interactions," Lab Chip **18**(9), 1298–1309 (2018).
11. P. S. Hiemstra, G. Grootaers, A. M. van der Does, C. A. M. Krul, and I. M. Kooter, "Human lung epithelial cell cultures for analysis of inhaled toxicants: Lessons learned and future directions," Toxicol. In Vitro **47**, 137–146 (2018).
12. S. Castellani, S. Di Gioia, L. di Toma, and M. Conese, "Human Cellular Models for the Investigation of Lung Inflammation and Mucus Production in Cystic Fibrosis," Anal. Cell. Pathol. **2018**, 1–15 (2018).
13. K. H. Benam, M. Mazur, Y. Choe, T. C. Ferrante, R. Novak, and D. E. Ingber, "Human Lung Small Airway-on-a-Chip Protocol," Methods Mol. Biol. **1612**, 345–365 (2017).
14. K. L. Sellgren, E. J. Butala, B. P. Gilmour, S. H. Randell, and S. Grego, "A biomimetic multicellular model of the airways using primary human cells," Lab Chip **14**(17), 3349–3358 (2014).
15. V. Mutyam, E. F. Libby, N. Peng, D. Hadjiliadis, M. Bonk, G. M. Solomon, and S. M. Rowe, "Therapeutic benefit observed with the CFTR potentiator, ivacaftor, in a CF patient homozygous for the W1282X CFTR nonsense mutation," J. Cystic Fibrosis **16**(1), 24–29 (2017).
16. S. E. Birket, K. K. Chu, L. Liu, G. H. Houser, B. J. Diephuis, E. J. Wilsterman, G. Dierksen, M. Mazur, S. Shastry, Y. Li, J. D. Watson, A. T. Smith, B. S. Schuster, J. Hanes, W. E. Grizzle, E. J. Sorscher, G. J. Tearney, and S. M. Rowe, "A functional anatomic defect of the cystic fibrosis airway," Am. J. Respir. Crit. Care Med. **190**(4), 421–432 (2014).
17. X. Liu, V. Ory, S. Chapman, H. Yuan, C. Albanese, B. Kallakury, O. A. Timofeeva, C. Nealon, A. Dakic, V. Simic, B. R. Haddad, J. S. Rhim, A. Dritschilo, A. Riegel, A. McBride, and R. Schlegel, "ROCK inhibitor and feeder cells induce the conditional reprogramming of epithelial cells," Am. J. Pathol. **180**(2), 599–607 (2012).
18. B. Prabhakarpandian, Y. Wang, A. Rea-Ramsey, S. Sundaram, M. F. Kiani, and K. Pant, "Bifurcations: focal points of particle adhesion in microvascular networks," Microcirculation **18**(5), 380–389 (2011).
19. M. Jarvis, M. Arnold, J. Ott, K. Pant, B. Prabhakarpandian, and S. Mitragotri, "Microfluidic co-culture devices to assess penetration of nanoparticles into cancer cell mass," Bioeng. Transl. Med. **2**(3), 268–277 (2017).
20. A. S. Shantanu Pradha, Charles J. Garson, Iman Hassani, Kapil Pant, Robert D. Arnold, Balabhaskar Prabhakarpandian, and Elizabeth A. Lipke, "Microfluidic cancer-on-a-chip platform for assessing anti-cancer drug efficacies," *Annual AACR Meeting, New Orleans*, LA (2016).
21. F. Soroush, T. Zhang, D. J. King, Y. Tang, S. Deosarkar, B. Prabhakarpandian, L. E. Kilpatrick, and M. F. Kiani, "A novel microfluidic assay reveals a key role for protein kinase C delta in regulating human neutrophil-endothelium interaction," J. Leukocyte Biol. **100**(5), 1027–1035 (2016).
22. B. Prabhakarpandian, M. C. Shen, J. B. Nichols, C. J. Garson, I. R. Mills, M. M. Matar, J. G. Fewell, and K. Pant, "Synthetic tumor networks for screening drug delivery systems," J. Controlled Release **201**, 49–55 (2015).
23. G. Lamberti, B. Prabhakarpandian, C. Garson, A. Smith, K. Pant, B. Wang, and M. F. Kiani, "Bioinspired microfluidic assay for in vitro modeling of leukocyte-endothelium interactions," Anal. Chem. **86**(16), 8344–8351 (2014).
24. B. Prabhakarpandian, M. C. Shen, J. B. Nichols, I. R. Mills, M. Sidoryk-Wegrzynowicz, M. Aschner, and K. Pant, "SyM-BBB: a microfluidic Blood Brain Barrier model," Lab Chip **13**(6), 1093–1101 (2013).
25. B. Prabhakarpandian, M. C. Shen, K. Pant, and M. F. Kiani, "Microfluidic devices for modeling cell-cell and particle-cell interactions in the microvasculature," Microvasc. Res. **82**(3), 210–220 (2011).
26. A. Moonwiriyakit, M. Koval, and C. Muanprasat, "Pharmacological stimulation of G-protein coupled receptor 40 alleviates cytokine-induced epithelial barrier disruption in airway epithelial Calu-3 cells," Int. Immunopharmacol. **73**, 353–361 (2019).
27. H. R. Park, M. O'Sullivan, J. Vallarino, M. Shumyatcher, B. E. Himes, J. A. Park, D. C. Christiani, J. Allen, and Q. Lu, "Transcriptomic response of primary human airway epithelial cells to flavoring chemicals in electronic cigarettes," Sci. Rep. **9**(1), 1400 (2019).
28. W. Huang, H. Zhao, H. Dong, Y. Wu, L. Yao, F. Zou, and S. Cai, "High-mobility group box 1 impairs airway epithelial barrier function through the activation of the RAGE/ERK pathway," Int. J. Mol. Med. **37**(5), 1189–1198 (2016).
29. M. Wojtkowski, V. Srinivasan, T. Ko, J. Fujimoto, A. Kowalczyk, and J. Duker, "Ultrahigh-resolution, high-speed, Fourier domain optical coherence tomography and methods for dispersion compensation," Opt. Express **12**(11), 2404–2422 (2004).
30. L. Liu, K. K. Chu, G. H. Houser, B. J. Diephuis, Y. Li, E. J. Wilsterman, S. Shastry, G. Dierksen, S. E. Birket, M. Mazur, S. Byan-Parker, W. E. Grizzle, E. J. Sorscher, S. M. Rowe, and G. J. Tearney, "Method for quantitative study of airway functional microanatomy using micro-optical coherence tomography," PLoS One **8**(1), e54473 (2013).
31. M. R. West, D. J. Ferguson, V. J. Hart, S. Sanjar, and Y. Man, "Maintenance of the epithelial barrier in a bronchial epithelial cell line is dependent on functional E-cadherin local to the tight junctions," Cell Commun. Adhes. **9**(1), 29–44 (2002).
32. B. Saatian, F. Rezaee, S. Desando, J. Emo, T. Chapman, S. Knowlden, and S. N. Georas, "Interleukin-4 and interleukin-13 cause barrier dysfunction in human airway epithelial cells," Tissue Barriers **1**(2), e24333 (2013).

Biomedical Optics EXPRESS

33. G. Lamberti, Y. Tang, B. Prabhakarpandian, Y. Wang, K. Pant, M. F. Kiani, and B. Wang, "Adhesive interaction of functionalized particles and endothelium in idealized microvascular networks," Microvasc. Res. **89**, 107–114 (2013).
34. K. Okuda, G. Chen, D. B. Subramani, M. Wolf, R. C. Gilmore, T. Kato, G. Radicioni, M. Kesimer, M. Chua, H. Dang, A. Livraghi-Butrico, C. Ehre, C. M. Doerschuk, S. H. Randell, H. Matsui, T. Nagase, W. K. O'Neal, and R. C. Boucher, "Localization of Secretory Mucins MUC5AC and MUC5B in Normal/Healthy Human Airways," Am. J. Respir. Crit. Care Med. **199**(6), 715–727 (2019).
35. S. E. Birket, J. M. Davis, C. M. Fernandez, K. L. Tuggle, A. M. Oden, K. K. Chu, G. J. Tearney, M. V. Fanucchi, E. J. Sorscher, and S. M. Rowe, "Development of an airway mucus defect in the cystic fibrosis rat," JCI Insight **3**(1), 97199 (2018).
36. G. M. Solomon, R. Francis, K. K. Chu, S. E. Birket, G. Gabriel, J. E. Trombley, K. L. Lemke, N. Klena, B. Turner, G. J. Tearney, C. W. Lo, and S. M. Rowe, "Assessment of ciliary phenotype in primary ciliary dyskinesia by micro-optical coherence tomography," JCI Insight **2**(5), e91702 (2017).
37. V. Mirra, C. Werner, and F. Santamaria, "Primary Ciliary Dyskinesia: An Update on Clinical Aspects, Genetics, Diagnosis, and Future Treatment Strategies," Front. Pediatr. **5**, 135 (2017).
38. S. Irving, M. Dixon, M. R. Fassad, E. Frost, J. Hayward, K. Kilpin, S. Ollosson, A. Onoufriadis, M. P. Patel, J. Scully, S. B. Carr, H. M. Mitchison, M. R. Loebinger, C. Hogg, A. Shoemark, and A. Bush, "Primary Ciliary Dyskinesia Due to Microtubular Defects is Associated with Worse Lung Clearance Index," Lung **196**(2), 231–238 (2018).
39. C. M. Fernandez-Petty, G. W. Hughes, H. L. Bowers, J. D. Watson, B. H. Rosen, S. M. Townsend, C. Santos, C. E. Ridley, K. K. Chu, S. E. Birket, Y. Li, H. M. Leung, M. Mazur, B. A. Garcia, T. I. A. Evans, E. F. Libby, H. Hathorne, J. Hanes, G. J. Tearney, J. P. Clancy, J. F. Engelhardt, W. E. Swords, D. J. Thornton, W. P. Wiesmann, S. M. Baker, and S. M. Rowe, "A glycopolymer improves vascoelasticity and mucociliary transport of abnormal cystic fibrosis mucus," JCI Insight **4**(8), e125954 (2019).
40. X. M. Bustamante-Marin, W. N. Yin, P. R. Sears, M. E. Werner, E. J. Brotslaw, B. J. Mitchell, C. M. Jania, K. L. Zeman, T. D. Rogers, L. E. Herring, L. Refabert, L. Thomas, S. Amselem, E. Escudier, M. Legendre, B. R. Grubb, M. R. Knowles, M. A. Zariwala, and L. E. Ostrowski, "Lack of GAS2L2 Causes PCD by Impairing Cilia Orientation and Mucociliary Clearance," Am. J. Hum. Genet. **104**(2), 229–245 (2019).
41. L. Liu, S. Shastry, S. Byan-Parker, G. Houser, K. K. Chu, S. E. Birket, C. M. Fernandez, J. A. Gardecki, W. E. Grizzle, E. J. Wilsterman, E. J. Sorscher, S. M. Rowe, and G. J. Tearney, "An autoregulatory mechanism governing mucociliary transport is sensitive to mucus load," Am. J. Respir. Cell Mol. Biol. **51**(4), 485–493 (2014).
42. H. M. Leung, S. E. Birket, C. Hyun, T. N. Ford, D. Cui, G. M. Solomon, R. J. Shei, A. T. Adewale, A. R. Lenzie, C. M. Fernandez-Petty, H. Zheng, J. H. Palermo, D. Y. Cho, B. A. Woodworth, L. M. Yonker, B. P. Hurley, S. M. Rowe, and G. J. Tearney, "Intranasal micro-optical coherence tomography imaging for cystic fibrosis studies," Sci. Transl. Med. **11**(504), eaav3505 (2019).
43. S. P. Deosarkar, B. Prabhakarpandian, B. Wang, J. B. Sheffield, B. Krynska, and M. F. Kiani, "A Novel Dynamic Neonatal Blood-Brain Barrier on a Chip," PLoS One **10**(11), e0142725 (2015).
44. P. Kolhar, A. C. Anselmo, V. Gupta, K. Pant, B. Prabhakarpandian, E. Ruoslahti, and S. Mitragotri, "Using shape effects to target antibody-coated nanoparticles to lung and brain endothelium," Proc. Natl. Acad. Sci. U. S. A. **110**(26), 10753–10758 (2013).
45. S. Pradhan, A. M. Smith, C. J. Garson, I. Hassani, W. J. Seeto, K. Pant, R. D. Arnold, B. Prabhakarpandian, and E. A. Lipke, "A Microvascularized Tumor-mimetic Platform for Assessing Anti-cancer Drug Efficacy," Sci. Rep. **8**(1), 3171 (2018).
46. C. P. Blobel, "3D trumps 2D when studying endothelial cells," Blood **115**(25), 5128–5130 (2010).
47. C. O. Lizama and A. C. Zovein, "Polarizing pathways: balancing endothelial polarity, permeability, and lumen formation," Exp. Cell Res. **319**(9), 1247–1254 (2013).